ChemPubSoc Europe
DOI: 10.1002/batt.201900107
BATTERIES & SUPERCAPS
Articles

Ion-Selective Membrane-Free Dual Sulfur-Iodine Catholyte for Low-Cost and High-Power Flow Battery Applications

Wei Huang,[a] Qingli Zou,[a] and Yi-Chun Lu*[a]

Highly concentrated polysulfide- (PS) and iodide-based (I_3^-/I^-) redox couples are promising active materials for redox flow battery applications owing to their high volumetric capacity. However, their applications in lithium redox flow batteries suffer from severe shuttle of iodine and PS and thus require the use of an ion-selective ceramic membrane for stable operation. This inherent challenge critically limits the practical current density of the flow battery (<1 mA cm^{-2}). Herein, we developed a dual PS-LiI catholyte to simultaneously alleviate the shuttling of iodine and the passivation of Li_2S, demonstrating stable ion-selective membrane-free Li-catholyte cells achieving volumetric capacity between 30–60 Ah L$^{-1}_{catholyte}$ with long cycle life ($>$ 150 cycles) at high current densities (3.8 mA cm^{-2} and 5.4 mA cm^{-2}). The dual PS-LiI catholyte not only increases the volumetric capacity and stability, but also removes the resistive and high-cost ion-selective membrane for low-cost, high-energy and high-power flow battery applications.

1. Introduction

Electrochemical energy storage systems are critical for the integration of intermittent renewable energy sources (solar and wind) into modern smart grids.[1–4] Redox flow batteries (RFBs) are one of the most promising energy storage technologies for large-scale electricity storage, owing to design flexibility of decoupling power and energy capacity.[5–12] However, conventional RFBs suffer from low energy density, which strongly decreases their competitiveness for both stationary grid storage and transportation applications.[11–14]

One important approach to improve the energy density of RFBs is the concept of a hybrid flow battery using an alkaline metal (e.g. Li metal) coupled with aqueous cathodes,[15] such as ferricyanide,[16] $FeCl_3/FeCl_2$,[17] I_3^-/I^-[18–20] and aqueous polysulfide (PS),[21] separated by a glass ceramic membrane to prevent massive crossover. This unique concept combines the high solubility aqueous redox species and low reaction potential alkaline metals. However, the prominent bottlenecks of this approach are the safety issues from the incompatibility between aqueous solution and alkaline metals and the need for an expensive and highly resistive crack-free glass ceramic membrane. To address the incompatibility, non-aqueous Li-based flow batteries utilizing organic redox compounds as catholytes have been shown effective on increasing the power density, energy density and cycle life, such as TEMPO-based,[22,23] Quinones-based[24–26] and ferrocene-based[10,13,27–30] redox systems. However, the low solubility of organic redox compounds limited its energy density and the needs for ceramic membrane still prevents practical applications.

Highly concentrated polysulfide (PS) catholyte has also been demonstrated effective in increasing energy density of RFBs.[12,34,36–38] Fan et al. proposed a carbon-percolating conducting network, which realized a catholyte volumetric capacity of 117 Ah L^{-1}. To further increase the volumetric capacity, Chen et al. employed sulfur-impregnated carbon (S/C) composite as a flow cathode to achieve a catholyte volumetric capacity of 294 Ah L^{-1},[34] followed by introducing LiI as a redox active material (5 M LiI) in the Li–S flow catholyte, achieving a substantial increase in the Li–S capacity associated with Li_2S formation.[35] However, when the concentration of I_3^- increases, the I_3^--shuttle increases (Figure 1B), which requires the addition of solid-state ion-selective ceramic membrane (e.g. $Li_{1+x}Al_yGe_{2-y}(PO_4)_3$, LAGP or LICGC) to prevent the I_3^--shuttles in the system.[19,35,39,40] Such requirement significantly reduces the power capability of the flow battery owing to high interfacial

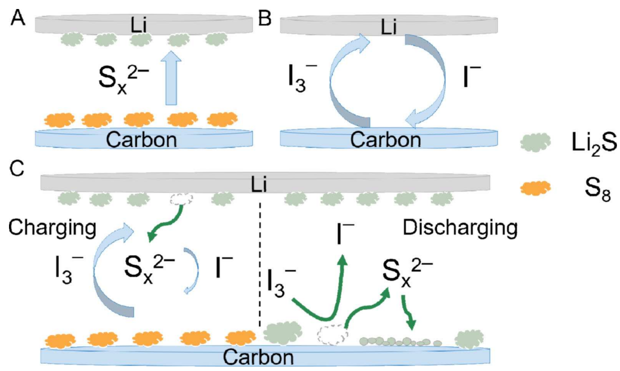

Figure 1. The schematic illustration of sulfur and iodine species during battery operation in (A) a Li/S cell where PS diffuses away and deposits on Li metal as Li_2S; (B) Li/iodine cell where I_3^- diffuses and reacts with Li metal vigorously, leading to continuous shuttling; (C) Li/PS–LiI dual catholyte cell where I_3^--shuttle current is reduced because of Li_2S deposition on the Li metal and PS is regenerated from Li metal after reacting with I_3^-.

[a] W. Huang, Q. Zou, Prof. Y.-C. Lu
Energy and Electrochemical Interfaces Laboratory
Department of Mechanical and Automation Engineering, Faculty of Engineering
The Chinese University of Hong Kong
Shatin, N.T. 999077, Hong Kong SAR (China)
E-mail: yichunlu@mae.cuhk.edu.hk

Supporting information for this article is available on the WWW under https://doi.org/10.1002/batt.201900107 resistance and ohmic resistance associated with solid-state electrolyte.[40–42] In addition to acting as a redox active material, LiI additives was also reported to improve Li–S batteries by forming a so-called "protective layer" to protect the active material particles from the direct contact with an organic electrolyte solvent and greatly suppress polysulfide dissolution.[42] Therefore, how to employ LiI as both redox active materials contributing capacity and promoter for polysulfide redox chemistry without needing resistive solid-state electrolyte is important for further advancement of the system. Furthermore, the underlying mechanism responsible for Li–S capacity enhancement and the impacts of dual redox system in the cathode and the Li anode are not well-understood.[37,42–46]

In this work, we investigate the chemical and electrochemical interactions between PS and I_3^- and exploit these interactions to reduce I_3^--shuttles without using resistive ion-selective ceramic membranes. This approach achieves a Li-catholyte cell with volumetric capacity between 30–60 Ah L^{-1} at high current density (3.8–5.4 mA cm^{-2}) for more than 150 cycles. Static and continuous Li-flow batteries were demonstrated with dual PS–LiI catholyte. Our work provides in-depth mechanistic understanding of the synergistic interaction between PS and iodine redox active materials and exploits it for designing high-rate and high-energy-density redox flow batteries.

2. Results and Discussion

Our design strategy for a synergistic dual PS–LiI catholyte is illustrated in Figure 1C. With a proper ratio of S and I, the issues facing Li–S batteries (continuous PS dissolution & premature Li_2S passivation) and Li–I batteries (I_3^- shuttle) could be exploited as remedies for each other. In an ion-selective membrane-free Li/PS–LiI dual catholyte cell, some PS will inevitably diffuse to Li anode and deposits on the Li metal forming Li_2S particles (Figure 1A and Figure 1C). During charging, I^- is oxidized to I_3^- in the cathode, which diffuses to the anode side. Instead of reacting rapidly with Li metal in a PS-free system (as shown in Figure 1B), the I_3^- will react with Li_2S on the Li surface to form PS and iodide via Equation (1):

$$3\,LiI_3 + 4\,Li_2S \rightarrow 9\,LiI + Li_2S_4 \tag{1}$$

In this case, part of the Li_2S deposits on the Li anode are regenerated and released back to the cathode; meanwhile, the shuttle current of I_3^- is reduced compared to a PS-free cell because I_3^- reacts slower with Li_2S than with Li metal (Figure 1C). During discharging, the trace of I_3^- in the cathode will oxidize solid Li_2S to form soluble PS, which can be further reduced in the cathode. We hypothesize that this process will delay the passivation of solid Li_2S in the cathode thereby increasing the discharge capacity of Li–S batteries. Electrochemical, spectroscopic and morphological characterizations were conducted to probe and verify these hypotheses and design considerations.

2.1. The Presence of PS in Suppressing Triiodide Shuttling

We examined the electrochemical behaviors of the Li/PS–I dual catholyte cells in direct comparison with individual Li–PS and Li–I cells. Carbon paper current collector and porous separators were used in Li-half cells (see Experimental). We compare pure Li–PS cell (0.375 M nominally "Li_2S_8"), pure Li-LiI cell (1 M) and Li/PS–LiI dual catholyte cells (0.375 M "Li_2S_8"-1 M LiI) in 0.2 M $LiClO_4$/0.1 M $LiNO_3$ in DOL:DME. The full galvanostatic voltage profiles are shown in Figure S1A & B and they are separated by charge and discharge steps in the main figure for clarity.

Figure 2A shows the first charging profile of the pure LiI, pure PS and the dual PS–LiI catholyte cell to 2.8 V or 3.2 V at 0.15 mA cm^{-2}. For the pure LiI cell, the charging capacity is significantly higher than the theoretical capacity of I^-/I_2 (1.34 mAh), which confirms the severe shuttle effect of the I_3^- in the LiI-alone system. The charging profiles of the dual PS–LiI catholyte cell contain charging plateau of S_8^{2-}/S_8 (~2.4 V) and the charging plateau of I^-/I_3^- (2.8–3.0 V). In contrast to the severe shuttle capacity observed in the single LiI system (as shown by the never ending charging plateau), the charge plateau of I^-/I_3^- in dual PS–LiI catholyte cell (charged to 3.2 V) showed a sharp voltage ending with a charge capacity of 1.285 mAh, which is slightly higher than the theoretical capacity (0.895 mAh, I^-/I_3^-), achieving a coulombic efficiency of 70%. Although only porous Celgard separators are employed in these cells, the severe shuttle effect of I^-/I_3^- was significantly reduced simply with the presence of PS in the electrolyte. As discussed in Figure 1C, the reduction of I_3^--shuttle can be attributed to the protection of PS deposits on the Li anode. To verify this hypothesis, we pre-treated a Li anode with PS solution (see Experimental) and employed it as the Li anode in a pure LiI system, denoting "psLi–LiI" cell. As shown in Figure 2B, the I_3^- shuttle was effectively reduced when using the Li anode pre-treated with PS solution, confirming our hypothesis of the enhanced mechanism on reducing I_3^--shuttling. Interestingly, some discharge capacity associated with PS was observed in the psLi–LiI cell (below 2.4 V) even though no PS was added in the cathode, confirming that the S–containing deposits on the Li anode can be oxidized by I_3^- and be regenerated back to cathode (equation 1). These experimental evidences support our hypothesis on constructing a synergistic dual PS–LiI system to suppress I_3^--shuttle and regenerate the lost PS from the Li anode.

2.2. The Effect of Triiodide on Increasing Sulfur Utilization-Dissolve/Re-deposit Mediation

After the charging steps (Figure 2A), all the cells were subsequently discharged at 0.15 mA cm^{-2}. To directly compare the sulfur utilization at different conditions, the voltage profile below 2.4 V is shown in Figure 2C. Interestingly, the dual PS–LiI catholyte cell (pre-charged to 3.2 V) delivered the highest sulfur capacity (1295 mAh g$_s^{-1}$), followed by the dual PS–LiI catholyte cell charged to 2.8 V (1039 mAh g$_s^{-1}$), followed by the pure S cell charged to 3.2 V (919 mAh g$_s^{-1}$). The discharge capacity of

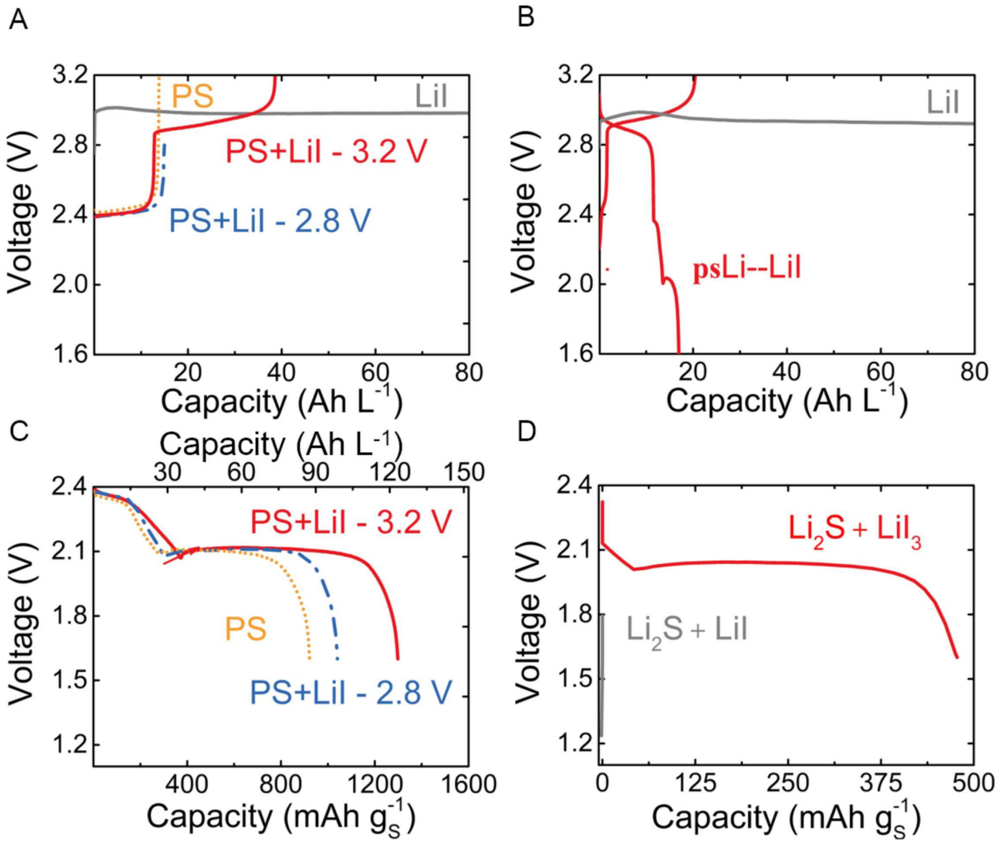

Figure 2. Charge-discharge voltage profiles of PS and iodide systems. All the cells are operated at 0.15 mA cm^{-2}. (A) Charge voltage profiles of the first cycle of PS (0.375 M Li_2S_8; charged to 3.2 V), LiI (1 M), and PS (0.375 M Li_2S_8) + LiI (1 M) charged to 2.8 V or 3.2 V. (B) Charge-discharge voltage profiles of LiI (1 M) with PS-treated Li anode (psLi) in comparison with untreated Li metal. (C) Discharge voltage profiles of S specific capacities of the first cycle of PS (0.375 M Li_2S_8) and PS (0.375 M Li_2S_8) + LiI (1 M) catholytes (charged to 2.8 V or 3.2 V). (D) Discharge voltage profiles of Li_2S particles (2.3 mg) in the presence of LiI (1 M, 50 μL, grey line) or LiI_3 (0.333 M, 50 μL, red line).

the first plateau (>2.1 V) was similar in all cases (~160 mAh g_s^{-1}) and the capacity differences mainly originated from the second discharge plateau, which is associated with PS reduction to form solid Li_2S.

The increases of sulfur capacity at the second discharge plateau can be attributed to (1) some PS was regenerated from the anode after reacting with I_3^- (eq. 1) as demonstrated in Figure 2B; (2) the trace of I_3^- in the cathode could oxidize solid Li_2S formed during discharge to soluble PS, which then can be reduced again in cathode. Such dissolve and re-deposit process could alter the morphology of Li_2S to avoid premature electrode passivation (improved S utilization).[37] To probe the second hypothesis, we manually mixed solid Li_2S powder with LiI or LiI_3 and discharge the mixture in the Li-half cell. As shown in Figure 2D, when Li_2S is mixed with I_3^-, the mixture can deliver a discharge capacity at ~2.05 V (500 mAh g_s^{-1}), which confirms that I_3^- can oxidize Li_2S to generate PS and deliver capacity. This means that when solid Li_2S is formed during PS reduction, the trace of I_3^- in the solution would oxidize Li_2S to PS until all the I_3^- is reduced to I^-, which cannot further react with Li_2S (Figure 2D, grey line). Figure S1C shows the coulombic efficiency (CE) of PS-LiI dual electrolyte charged to 2.8 V and 3.2 V in comparison with pure PS. The CE is the highest for PS-LiI charged to 2.8 V (95%) followed by PS-LiI charged to 3.2 V (90%) and pure PS (79%). The CE for pure LiI is 0% as continuous charging was observed (shuttling). This suggests that introducing the reaction between Li_2S and I_3^- significantly improves the CE of both LiI reactions and PS reactions. UV-vis spectroscopy and mass spectroscopy support that PS is formed after mixing Li_2S with LiI_3, as shown in Figure S2 and Figure S3, respectively. Based on the discharge capacity obtained from $Li_2S + LiI_3$ mixture (500 mAh g_s^{-1}, Figure 2D), the reaction between Li_2S and LiI_3 could generate Li_2S_4 following Equation (2):

$$4\ Li_2S + 3\ LiI_3 \rightarrow Li_2S_4 + 9\ LiI \quad (2)$$

followed by reduction of Li_2S_4 to Li_2S (theoretically 628 mAh g_s^{-1}; Equation (3)):

$$Li_2S_4 + 6\ e^- + 6\ Li^+ \rightarrow 4\ Li_2S \quad (3)$$

One potential question is whether the oxidized phase I_3^- is still present during cell discharge to low voltages. We exploited UV-Vis spectroscopy (see EXPERIMENTAL PROCEDURES and Figure S4) to show that when the cell discharged to 2.3 V (Figure S4A), the I_3^- absorbance (366 nm)[46] of the dual PS–LiI electrolyte that was pre-charged to 3.2 V is much higher than that of the PS electrolyte pre-charged to 3.2 V. When the cell discharged to 2.1 V (Figure S4B), the I_3^- absorbance is similar in all cases. This suggests that the trace amount of I_3^- was present in the dual electrolyte at 2.3 V but diminished when discharge to 2.1 V. The higher amount of I_3^- found in the dual electrolyte pre-charged to 3.2 V compared to that pre-charged to 2.8 V is consistent with the higher discharge capacity achieved when charged to 3.2 V (Figure 2C) owing to higher concentration of I_3^-. To quantify the capacity enhancement solely from the effect of I_3^- on PS reactions in cathode, we inserted one solid-state electrolyte (LAGP) to fully decouple the cathode from the anode (so no PS can be diffused back to the cathode). Figure S5 shows that the presence of I^-/I_3^- (charged to 3.2 V) increased the Li–S discharge capacity at the second plateau for ~200 mAh g_s^{-1} even when eliminating the cross-talk between cathode and anode. Cyclic voltammograms (CVs) (Figure S6) show that the peak currents, reversibility and peak separation of both PS and LiI redox reactions in the dual PS–LiI catholyte improved from the pure PS and pure LiI system.

2.3. Morphology of the Electrodes

To evaluate how I_3^- affects the morphology of Li_2S, we examine morphological changes of both cathode and anode after cycling in pure S and dual PS–LiI catholytes. Figure 3 shows the SEM image of the electrodes cycled in pure S-system and in dual PS–LiI catholyte at the fully discharge state. In the pure PS system, the cycled PS electrode contains large size of aggregates in the order of 5–10 µm (Figure 3A). These aggregates could be attributed to solid Li_2S accumulated upon cycling as supported by X-ray diffraction (XRD) patterns (Figure S7) and Energy-dispersive X-ray spectroscopy (EDS) mapping (Figure S8A) showing less S density in the EDS mapping. The cycled Li electrode in the pure PS system show solid aggregates on the surface (Figure 3B), which contains S element as evidenced from EDS mapping (Figure S9A). The formation of S-containing aggregates on the Li electrode confirms that PS diffused to anode and deposited on the Li surface.

In contrast, in the dual PS–LiI catholyte, the cycled PS electrode show much smaller Li_2S particles with more open pores instead of large Li_2S aggregates (Figure 3C and Figure S8B). This supports that the presence of I_3^- changes the morphology of Li_2S accumulated in the S electrode, transforming thick and large insulating aggregates to thin and small particles. Interestingly, we observed many open holes on the Li surface in the dual PS–LiI catholyte (Figure 3D). We believe that the holes on Li surface represent the area where S-containing aggregates are oxidized by I_3^- to soluble PS (PS regeneration). This hypothesis is further supported by the EDS mapping of the Li anode where the S content is clearly lower inside the hole than the edge of the hole (Figure S9B).

2.4. Ion-Selective Membrane-Free Batteries Enabled by Dual PS–LiI Catholyte

Based on our discussion above, the dual PS–LiI system alleviates continuous shuttling of I_3^-, regenerates PS from Li anode and improves the Li_2S deposition morphology. To balance the flux of both species, the ratio between S and I in the dual PS–LiI catholyte is an important factor determining the effectiveness of I_3^- shuttle suppression and the PS-utilization. According to the design consideration (Figure 1), insufficient PS relative to I will not effectively suppress I_3^- shuttle[37] while insufficient I relative to PS cannot effectively improve S utilization. When the relative content of I is high (e.g. S:I = 1:3), severe shuttle of I_3^- occurs (Figure S10) due to

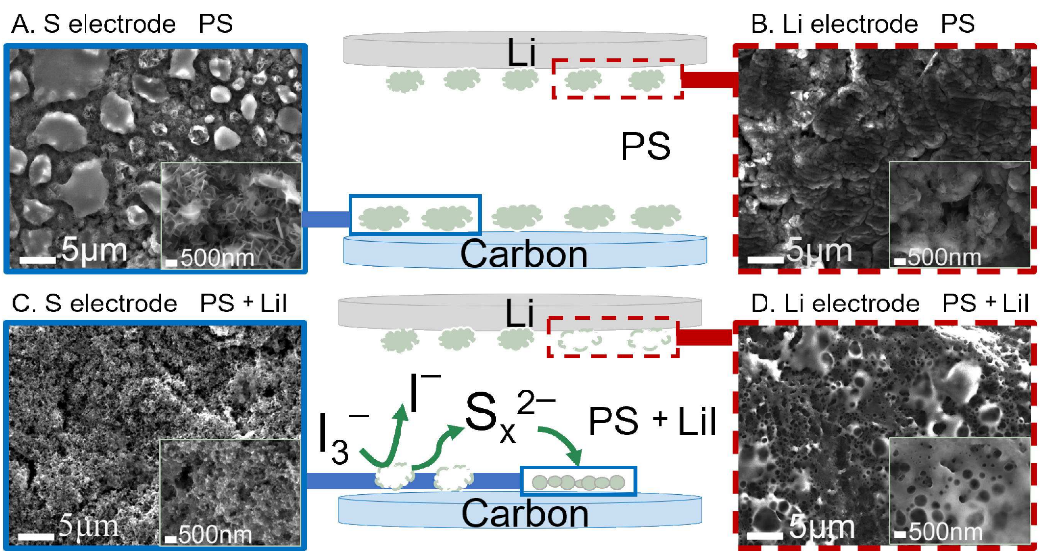

Figure 3. The SEM images of positive electrodes (S electrode) and Li negative electrodes cycled for 10 times at 0.15 mA cm^{-2} (all the cells were stopped at the discharged state). (A) Sulfur electrode on carbon paper cycled in PS (0.375 M Li_2S_8) catholyte; (B) Li electrode cycled in PS (0.375 M Li_2S_8) catholyte; (C) Sulfur electrode on carbon paper cycled in PS (0.375 M Li_2S_8) + LiI (1 M) catholyte; (D) Li electrode cycled in PS (0.375 M Li_2S_8) + LiI (1 M) catholyte. All the scale bars of the images and insertions are 5 µm and 500 nm, respectively.

insufficient PS deposit at the Li anode to prevent reactions between I_3^- and Li anode. When the relative content of PS increased to a S:I ratio of 1:2, the first cycle of I_3^--shuttle was suppressed (Figure S10), but not the 2nd cycle (Figure S10). This suggests that the S-containing deposits on the Li anode are consumed and the concentration of PS is not high enough to form stable S-containing deposits on the Li surface. After further increase in relative PS content to a S:I ratio of 1:1 or higher, the severe I_3^- shuttle can be effectively suppressed as indicated by the sharp termination of the charging voltage for S:I ratios of 1:1 (Figure S10).

We compare the cycling stability and rate capability of dual PS–LiI catholyte (0.125 M Li_2S_8 + 1 M LiI, S:I = 1:1) along with pure PS (0.125 M Li_2S_8) and LiI (1 M) in Figure 4. Full cycling profiles at different current densities of the pure PS, pure LiI and dual PS–LiI catholytes are shown in Figure S11 and Figure S12. Figure 4A shows the S specific discharge capacity as a function of cycle number at various current densities. Clearly, the dual PS–LiI catholyte exhibits significantly higher S discharge capacity and higher rate capability upon cycling than the pure PS system. The I part in dual PS–LiI catholyte shows a continuously cycling while the pure LiI system shows quick fading and severe shuttle effect (Figure 4B). The CE of pure LiI system gradually turned to zero owing to severe shuttle effect (Figure S13). The synergistic effect is also prominently observed in elevated concentrations. We increase the concentration of PS and LiI to 0.5 M Li_2S_8 + 4 M LiI (S:I = 1:1) and evaluate the battery performance of the highly-concentrated catholyte. As shown in Figure S14, a volumetric capacity of 166 Ah L^{-1} can be achieved with improved cycle life compared to the pure PS and pure LiI system. The utilization ratio of S and I maintains ~60% and 50% in the dual system, respectively, whereas only 50% was achieved in pure PS and 0% in pure LiI catholyte (Figure S14). When the current density increased to

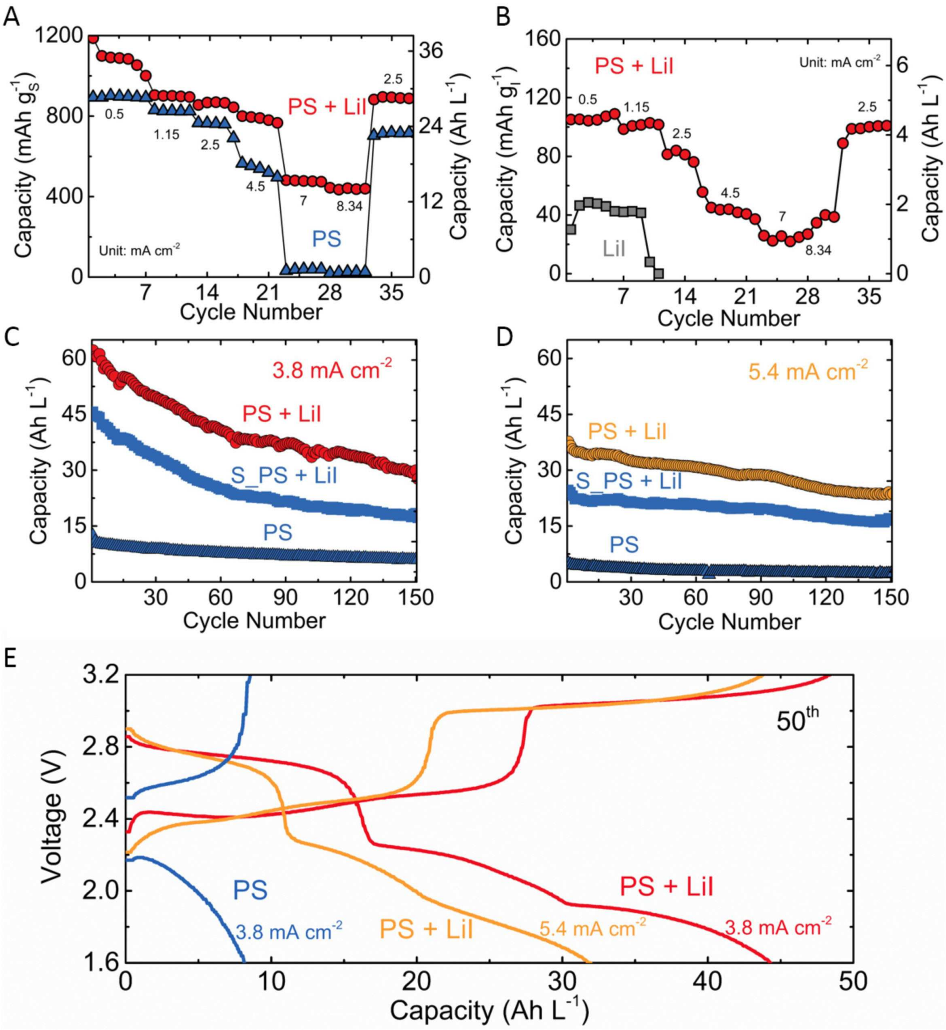

Figure 4. Electrochemical characterization of dual PS–LiI catholyte in comparison with pure PS and LiI catholyte. (A) Cycling and rate capability of specific S capacity of pure PS (0.125 M Li_2S_8) and dual PS–LiI catholyte (0.125 M Li_2S_8 + 1.0 M LiI) S part. (B) Cycling and rate capability of specific I capacity of pure LiI (1 M) and dual PS–LiI catholyte (0.125 M Li_2S_8 + 1.0 M LiI; I part). (C) Cycling and rate capability of total capacity (red) and S part of PS (0.5 M Li_2S_8) + LiI (4 M; light blue) and PS (0.5 M Li_2S_8; dark blue) catholytes at 3.8 mA cm^{-2} (S-based 2 C). (D) Cycling and rate capability of total capacity (yellow) and S part of PS (0.5 M Li_2S_8) + LiI (4 M; light blue) and PS (0.5 M Li_2S_8; dark blue) catholytes at 5.4 mA cm^{-2} (S-based 2 C). (E) Galvanostatic voltage profiles of pure PS (0.5 M Li_2S_8) catholyte at 3.8 mA cm^{-2} and PS (0.5 M Li_2S_8) + LiI (4 M) catholyte at 3.8 mA cm^{-2} and 5.4 mA cm^{-2} at 50th cycle.

3.8 mA cm^{-2} (equivalent 2 C based on sulfur) and 5.4 mA cm^{-2}, the dual system delivered a much higher volumetric capacity than the pure PS system, as shown in Figure 4C and Figure 4D. The capacity retention of the I part of the dual system in comparison to the pure LiI system is shown in Figure S15, showing consistent improvement of dual electrolyte over the pure LiI system. Figure 4E shows the galvanostatic voltage profiles of dual PS–LiI catholyte in comparison with pure PS system, exhibiting the synergistic improvement on both S and I capacities. Finally, a ion-selective membrane-free Li–flow cell with the designed dual PS–LiI catholyte was demonstrated for flow battery applications[34,35] (Figure S16), showing a significantly reduced I_3^--shuttle compared to the pure LiI flow battery.

3. Conclusion

Ion-selective membrane-free dual PS–LiI catholytes are achieved by exploiting synergistic interactions between PS and I. The dual PS–LiI catholyte was found to effectively suppress I_3^- shuttle via reacting with S-containing deposit on the Li anode and increase the cathode capacity with the PS regenerated from the anode. On cathode, the "dissolve and re-deposit" process of PS caused by the chemical reaction between I_3^- and solid Li_2S avoids formation of large Li_2S aggregates and thus improves the S utilization. The dual PS–LiI catholyte achieves a PS utilization improvement and enabled volumetric capacity between 30–60 Ah L$^{-1}_{catholyte}$ at high current densities (3.8–5.4 mA cm^{-2}) for more than 150 cycles. Our work provides in-depth mechanistic understanding of the synergistic interaction between PS and iodine redox active materials and enable the use of highly concentrated PS and iodide active materials without the protection of ion-selective membrane for low-cost, high-rate and high-energy-density flow battery applications. Future work on addressing the insoluble nature of PS discharge product and balancing the flux of both species with optimum coulumbic and energy efficiency are important for the further development of dual PS–LiI electrolyte.

Experimental Section

Preparation of Catholytes

All the catholytes were prepared with specific background solution of 0.1 M $LiNO_3$ and 0.2 M $LiClO_4$ in DOL:DME (volume ratio = 1:1) to ensure the basic conductivity of the electrolyte. The LiI concentrations in catholytes were 0.33 M, 1 M, 2 M, 3 M and 4 M PS (Li_2S_8) was prepared through a chemical reaction between sulfur and lithium sulfide in the solution and used as the active materials of PS solution. The concentration was calculated by the amount of S atom. 0.125 M to 0.375 M "Li_2S_8" catholytes were prepared and the controlled experiment was done by 50 μL solution of the group of PS (0.375 M Li_2S_8) and PS (0.375 M Li_2S_8) + LiI (1 M). To find the optimal ratio of S and I, the ratios of S:I = 1:1, 1:2, 1:3, 2:1, 3:1, 4:1 and 5:1 were selected for the first cycle (charge first, then discharge). The catholytes used in high volumetric capacity catholyte were 0.5 M "Li_2S_8" + 4 M LiI and high C-rate application were 0.125 M "Li_2S_8" + 1 M LiI. To scale up the balance ratio, 0.5 M Li_2S_8 solution was fabricated. After the Li_2S_8 was fully generated, 4 M LiI solution was fabricated with 0.5 M Li_2S_8 solution.

Electrochemical Pre-Treatment of Li

The Li metal foils were treated in a symmetric cell with 50 μL 0.125 M Li_2S_8 DOL:DME solution as electrolyte under the current density of 0.15 mA cm^{-2} and active capacity of 4 mAh cm^{-2}. Then both Li metal foils were taken out and dried in vacuum. The Li foils are stood by to be prepared to construct a Li–iodine cell.

Static Cell Assembly and Electrochemical Measurement

The 2032-type coin cells were fabricated for the static tests and electrochemical measurement. Simple carbon papers with diameter of 16 mm (Fuel Cell The Earth) were used as cathode host material, with the addition of 50 μL catholyte, to construct a two-electrode configuration. Celgards were used as the separators of the cells. The system is also composed of a lithium metal foil as anode, a stainless-steel plate and a stainless-steel shrapnel. Galvanostatic experiments were performed with the multi-channel battery testers (LAND). Current density was calculated based on the effective geometric surface area of carbon paper. A constant current density of 0.15 mA cm^{-2} was applied to the cells, while the voltage range was set from 1.6 to 3.2 V_{Li}. The first cycle was chosen to compare the capacities of different conditions to avoid the historical effect. In the test of high volumetric capacity catholyte, 10 μL catholyte was added on the carbon paper with a diameter of 10 mm or 12 mm to justify the appropriate loading and current density and the Celgards were moistened with the same volume of background DOL/DME electrolyte as the added catholyte before assembling the cells.[37]

Li–Flow Cell Assembly and Electrochemical Measurement

The structure of the Li-flow cell was consistent with our previous works.[33,37]One piece of thin lithium foil was placed on the copper cell body, followed by one Celgard 2325 separator. A Teflon channel spacer (1 mm thickness) was placed between the lithium foil and a piece of pressed nickel foam, which was attached to an outer Al cell body fixed by six bolts. The catholyte was pumped into the channel by two cones. All the process was conducted in an Ar-filled glove box (Etelux, < 0.1 ppm H_2O and < 0.1 ppm O_2). The voltage window of the flow cell was set between 1.6 V and 3.2 V, with a limitation on charging or discharging time in 3 hours. The flow rate was between 3.5 mL min^{-1} and 5 mL min^{-1}.

The Preparation of UV-Vis Spectroscopy

The UV-Vis spectroscopic (SEC2000; ALS; Japan) was switched on for 30 min before the test. The darkness and reference were measured every time when change the samples. All the catholytes were diluted to 1/1500 for taking the UV-Vis test. The ex-situ UV-vis spectra were collected by well controlling the concentration of the detected catholytes. 50 μL Li_2S_8 (0.125 M) and Li_2S_8 (0.125 M) + LiI (1 M) catholytes were discharged to 2.3 V and the middle of second S-discharge plateau (around 2.1 V) after charging to 3.2 V in battery cell (to avoid the loss of active species). After discharging, the cathodes were taken out and immersed into 4 mL DOL:DME solvent for 15 min to solute the active species. Then the catholytes were taken out for UV-vis spectra collection.

Acknowledgements

The work described in this paper was fully supported by a grant from the Research Grant Council of the Hong Kong Special Administrative Region, China (Project No. T23-601/17-R). We thank Dr. Zhuojian Liang for his assistance of designing the cells. We also appreciate the assistance of Dr. Yucun Zhou and Jing Xie in the fabrication of solid electrolyte (LAGP).

Conflict of Interest

The authors declare no conflict of interest.

Keywords: catholyte · iodide · membrane-free · polysulfide · redox flow batteries

[1] B. Dunn, H. Kamath, J.-M. Tarascon, *Science* **2011**, *334*, 928.
[2] C. J. Barnhart, M. Dale, A. R. Brandt, S. M. Benson, *Energy Environ. Sci.* **2013**, *6*, 2804.
[3] J. Liu, J.-G. Zhang, Z. Yang, J. P. Lemmon, C. Imhoff, G. L. Graff, L. Li, J. Hu, C. Wang, J. Xiao, G. Xia, V. V. Viswanathan, S. Baskaran, V. Sprenkle, X. Li, Y. Shao, B. Schwenzer, *Adv. Funct. Mater.* **2013**, *23*, 929.
[4] K. Wang, K. Jiang, B. Chung, T. Ouchi, P. J. Burke, D. A. Boysen, D. J. Bradwell, H. Kim, U. Muecke, D. R. Sadoway, *Nature* **2014**, *514*, 348.
[5] F. Pan, Q. Wang, *Molecules* **2015**, *20*.
[6] K. Gong, Q. Fang, S. Gu, S. F. Y. Li, Y. Yan, *Energy Environ. Sci.* **2015**, *8*, 3515.
[7] Q. Huang, Q. Wang, *ChemPlusChem* **2015**, *80*, 312.
[8] Y. Zhao, Y. Ding, Y. Li, L. Peng, H. R. Byon, J. B. Goodenough, G. Yu, *Chem. Soc. Rev.* **2015**, *44*, 7968.
[9] M. Park, J. Ryu, W. Wang, J. Cho, *Nat. Rev. Mater.* **2016**, *2*, 16080.
[10] G. Cong, Y. Zhou, Z. Li, Y.-C. Lu, *ACS Energy Lett.* **2017**, *2*, 869.
[11] R. Yan, Q. Wang, *Adv. Mater.* **2018**, *30*, 1802406.
[12] Z. Wang, L.-Y. S. Tam, Y.-C. Lu, *Joule*.
[13] S. Evers, T. Yim, L. F. Nazar, *J. Phys. Chem. C* **2012**, *116*, 19653.
[14] Y. Yang, G. Zheng, Y. Cui, *Energy Environ. Sci.* **2013**, *6*, 1552.
[15] X. Wei, L. Cosimbescu, W. Xu, J. Z. Hu, M. Vijayakumar, J. Feng, M. Y. Hu, X. Deng, J. Xiao, J. Liu, V. Sprenkle, W. Wang, *Adv. Energy Mater.* **2015**, *5*.
[16] S. Roe, C. Menictas, M. Skyllas-Kazacos, *J. Electrochem. Soc.* **2016**, *163*, A5023.
[17] Y. Lu, J. B. Goodenough, Y. Kim, *J. Am. Chem. Soc.* **2011**, *133*, 5756.
[18] Y. Lu, J. B. Goodenough, *J. Mater. Chem.* **2011**, *21*, 10113.
[19] Y. Wang, Y. Wang, H. Zhou, *ChemSusChem* **2011**, *4*, 1087.
[20] Y. Zhao, H. R. Byon, *Adv. Energy Mater.* **2013**, *3*, 1630.
[21] Y. Zhao, L. Wang, H. R. Byon, *Nat. Commun.* **2013**, *4*, 1896.
[22] M. Yu, W. D. McCulloch, D. R. Beauchamp, Z. Huang, X. Ren, Y. Wu, *J. Am. Chem. Soc.* **2015**, *137*, 8332.
[23] N. Li, Z. Weng, Y. Wang, F. Li, H.-M. Cheng, H. Zhou, *Energy Environ. Sci.* **2014**, *7*, 3307.
[24] X. Wei, W. Xu, M. Vijayakumar, L. Cosimbescu, T. Liu, V. Sprenkle, W. Wang, *Adv. Mater.* **2014**, *26*, 7649.
[25] K. Takechi, Y. Kato, Y. Hase, *Adv. Mater.* **2015**, *27*, 2501.
[26] H. Senoh, M. Yao, H. Sakaebe, K. Yasuda, Z. Siroma, *Electrochim. Acta* **2011**, *56*, 10145.
[27] Y. Ding, G. Yu, *Angew. Chem. Int. Ed.* **2016**, *55*, 4772.
[28] Y. Ding, Y. Li, G. Yu, *Chem* **2016**, *1*, 790.
[29] B. Hwang, M.-S. Park, K. Kim, *ChemSusChem* **2015**, *8*, 310.
[30] Y. Ding, Y. Zhao, G. Yu, *Nano Lett.* **2015**, *15*, 4108.
[31] H. Kim, T. Yoon, Y. Kim, S. Hwang, J. H. Ryu, S. M. Oh, *Electrochem. Commun.* **2016**, *69*, 72.
[32] Y. Ding, Y. Zhao, Y. Li, J. B. Goodenough, G. Yu, *Energy Environ. Sci.* **2017**, *10*, 491.
[33] H. Chen, Q. Zou, Z. Liang, H. Liu, Q. Li, Y.-C. Lu, *Nat. Commun.* **2015**, *6*, 5877.
[34] R. D. Rauh, K. M. Abraham, G. F. Pearson, J. K. Surprenant, S. B. Brummer, *J. Electrochem. Soc.* **1979**, *126*, 523.
[35] F. Y. Fan, W. H. Woodford, Z. Li, N. Baram, K. C. Smith, A. Helal, G. H. McKinley, W. C. Carter, Y.-M. Chiang, *Nano Lett.* **2014**, *14*, 2210.
[36] R. Steudel, T. Chivers, *Chem. Soc. Rev.* **2019**.
[37] H. Chen, Y.-C. Lu, *Adv. Energy Mater.* **2016**, *6*, 1502183.
[38] G. Nikiforidis, K. Tajima, H. R. Byon, *ACS Energy Lett.* **2016**, *1*, 806.
[39] F.-C. Liu, W.-M. Liu, M.-H. Zhan, Z.-W. Fu, H. Li, *Energy Env. Sci* **2011**, *4*, 1261.
[40] Y. Zhou, Z. Li, Y.-C. Lu, *Nano Energy* **2017**, *39*, 554.
[41] J. C. Bachman, S. Muy, A. Grimaud, H.-H. Chang, N. Pour, S. F. Lux, O. Paschos, F. Maglia, S. Lupart, P. Lamp, L. Giordano, Y. Shao-Horn, *Chem. Rev.* **2016**, *116*, 140.
[42] F. Wu, J. T. Lee, N. Nitta, H. Kim, O. Borodin, G. Yushin, *Adv. Mater.* **2015**, *27*, 101.
[43] S. Meini, R. Elazari, A. Rosenman, A. Garsuch, D. Aurbach, *J. Phys. Chem. Lett.* **2014**, *5*, 915.
[44] H. Zhang, P. Zuo, J. Hua, Y. Ma, C. Du, X. Cheng, Y. Gao, G. Yin, *Electrochim. Acta* **2017**, *238*, 257.
[45] H.-J. Peng, J.-Q. Huang, X.-Y. Liu, X.-B. Cheng, W.-T. Xu, C.-Z. Zhao, F. Wei, Q. Zhang, *J. Am. Chem. Soc.* **2017**, *139*, 8458.
[46] Y. X. Ren, T. S. Zhao, M. Liu, Y. K. Zeng, H. R. Jiang, *J. Power Sources* **2017**, *361*, 203.

Manuscript received: July 29, 2019
Revised manuscript received: August 21, 2019
Accepted manuscript online: August 22, 2019
Version of record online: September 11, 2019